LEARNING TO ANNOTATE PART SEGMENTATION WITH GRADIENT MATCHING

Yu Yang
Department of Automation
Tsinghua University, BNRist
yang-yu16@mails.tsinghua.edu.cn

Xiaotian Cheng
Department of Automation
Tsinghua University, BNRist
cxt20@mails.tsinghua.edu.cn

Hakan Bilen
School of Informatics
University of Edinburgh
hbilen@ed.ac.uk

Xiangyang Ji
Department of Automation
Tsinghua University, BNRist
xyji@tsinghua.edu.cn

ABSTRACT

The success of state-of-the-art deep neural networks heavily relies on the presence of large-scale labelled datasets, which are extremely expensive and time-consuming to annotate. This paper focuses on tackling semi-supervised part segmentation tasks by generating high-quality images with a pre-trained GAN and labelling the generated images with an automatic annotator. In particular, we formulate the annotator learning as a learning-to-learn problem. Given a pre-trained GAN, the annotator learns to label object parts in a set of randomly generated images such that a part segmentation model trained on these synthetic images with their predicted labels obtains low segmentation error on a small validation set of manually labelled images. We further reduce this nested-loop optimization problem to a simple gradient matching problem and efficiently solve it with an iterative algorithm. We show that our method can learn annotators from a broad range of labelled images including real images, generated images, and even analytically rendered images. Our method is evaluated with semi-supervised part segmentation tasks and significantly outperforms other semi-supervised competitors when the amount of labelled examples is extremely limited.

1 INTRODUCTION

In recent years, deep neural networks have shown a remarkable ability to learn complex visual concepts from large quantities of labeled data. However, collecting manual annotations for a growing body of visual concepts remains an extremely expensive practice, especially for pixelwise prediction tasks such as semantic segmentation. A common and effective way of reducing the dependence on manual labels is first learning representations from unlabeled data (Pathak et al., 2016; Noroozi & Favaro, 2016; Gidaris et al., 2018; He et al., 2020) and then transferring learned representations to a supervised learning task (Chen et al., 2020; Zhai et al., 2019). The insight of this paradigm is that some of the transferred representations are informative, easily identified, and disentangled, such that small amount of labeled data suffices to train the target task.

A promising direction for learning such representations is using generative models (Kingma & Welling, 2014; Goodfellow et al., 2014), since they attain the capability of synthesizing photorealistic images and disentangling factors of variation in dataset. Recent methods (Goetschalckx et al., 2019; Shen et al., 2020; Karras et al., 2019; Plumerault et al., 2020; Jahanian et al., 2020; Voynov & Babenko, 2020; Spingarn-Eliezer et al., 2021; Härkönen et al., 2020) show that certain factors such as object shape and position in the images synthesized by generative adversarial networks (GANs) (Goodfellow et al., 2014) can be individually controlled by manipulating latent features. Building on the success of powerful GAN models, Zhang et al. (2021) and Tritrong et al. (2021) demonstrate that feature maps in StyleGAN (Karras et al., 2019; 2020b;a) can be mapped to semantic segmentation masks or keypoint heatmaps through a shallow decoder, denoted as *annotator* in this paper. Remarkably, the annotator

can be trained after few synthesized images are manually labeled, and the joint generator and trained annotator can be used as an infinite labeled data generator. Nonetheless, labeling synthesized images with "human in the loop" has two shortcomings: (i) it can be difficult to label the generated images of low quality; (ii) it requires continual human effort whenever the generator is changed.

To mitigate these limitations, one straightforward way is to inverse the generation process to obtain generator features for given images. In this way, annotator, which only receives as input generator features, can be trained from existing labeled data, not necessarily generated data. However, inversion methods can not ensure exact recovery of the generator features, leading to degraded performance of annotator (see Section C.1). Another way to address this issue is to align the joint distribution of generated images and labels with that of real ones using adversarial learning as in SemanticGAN (Li et al., 2021). However, adversarial learning is notoriously unstable (Brock et al., 2018) and requires large amount of data to prevent discriminator from overfitting (Karras et al., 2020a).

In this paper, we formulate the annotator learning as a learning-to-learn problem – the annotator learns to label a set of randomly generated images such that a segmentation network trained on these automatically labeled images obtains low prediction error on a small validation set of manually labeled images. This problem involves solving a nested-loop optimization, where the inner loop optimizes the segmentation network and the outer loop optimizes the annotator based on the solution of inner-loop optimization. Instead of directly using end-to-end gradient-based meta learning techniques (Li et al., 2019; Pham et al., 2021), we reduce this complex and expensive optimization problem into a simple gradient matching problem and efficiently solve it with an iterative algorithm. We show that our method obtains performance comparable to the supervised learning counterparts (Zhang et al., 2021; Tritrong et al., 2021) yet overcomes their shortcomings such that labeled data within a broader range including real data, synthetic data, and even out-of-domain data can be utilized.

Our method requires a large quantity of unlabeled data for pre-training GANs and a relatively small amount of labeled data for training annotator, which drops into a semi-supervised learning setting. Our method relies on unconditional GANs and hence is limited by their performance. As the state-of-the-art GANs only produce appealing results on single-class images but struggle to model complex scenes, we focus on part segmentation of particular classes and avoid segmentation of multi-object scenes.

Our contribution can be summarized as follows. (i) We formulate the learning of annotations for GAN-generated images as a learning-to-learn problem and propose an algorithm based on gradient matching to solve it. As a consequence, we achieve learning segmentation from synthetic labeled images and generalize to real images, even when there is domain gap between synthetic and real images. (ii) We empirically show that our method significantly outperforms other semi-supervised segmentation methods in the few-label regime.[1]

2 Related Work

Semi-supervised learning Semi-supervised learning (SSL) (Zhu, 2005) augments the training of neural networks from a small amount of labeled data with a large-scale unlabeled dataset. A rich body of work regularizes networks on unlabeled data with consistency regularization. In particular, networks are required to make consistent prediction over previous training iterations (Laine & Aila, 2017; Tarvainen & Valpola, 2017; Izmailov et al., 2018), noisy inputs (Miyato et al., 2018), or augmented inputs (Berthelot et al., 2019b;a; Sohn et al., 2020). This paradigm is also interpreted as a teacher-and-student framework where teacher produces pseudo labels for unlabelled data to supervise the training of students. Pseudo labels can be enhanced with heuristics (Lee et al., 2013; Berthelot et al., 2019a) or optimized towards better generalization (Pham et al., 2021; Li et al., 2019). Apart from image classification tasks, the above ideas are also successfully applied to semantic segmentation tasks (Hung et al., 2018; Ouali et al., 2020; Ke et al., 2020; French et al., 2020). Our work can also be interpreted from teacher-and-student perspective. In contrast to the above methods that adopt homogeneous network structures for teacher and student, our work employ generative models as teacher and discriminative models as student.

Other SSL approaches explore the utility of unlabelled data from representation learning perspective. In particular, deep neural networks are first optimized on the unlabeled data with self-supervised

[1]Code is available at https://github.com/yangyu12/lagm.

learning tasks (Pathak et al., 2016; Noroozi & Favaro, 2016; Gidaris et al., 2018; He et al., 2020) to gain powerful and versatile representations, and then finetuned on the labeled data to perform target tasks (Chen et al., 2020; Zhai et al., 2019). In addition, efficient and transferable representations can also be learned with generative models that are typically trained without labels. To this end, one promising direction is to decode generative features into dense annotations such as segmentation masks and keypoint heatmap to facilitate SSL, as done in SemanticGAN (Li et al., 2021), Dataset-GAN (Zhang et al., 2021), RepurposeGAN (Tritrong et al., 2021) and our work. However, our work differs from these works in the way that we formulate the annotator learning as a learning-to-learn problem which is solved with gradient matching. Particularly, unlike SemanticGAN (Li et al., 2021) that learns annotator and data generator jointly, our method presumes a fixed pre-trained GAN and learns annotator only, which circumvents the complication of joint learning.

Semantic Part Segmentation Semantic part segmentation, which decomposes rigid or non-rigid objects into several parts, is of great significance in tremendous computer-vision tasks such as human parsing (Dong et al., 2014; Nie et al., 2018; Fang et al., 2018; Gong et al., 2017), pose estimation (Yang & Ramanan, 2011; Shotton et al., 2011; Xia et al., 2017) and 3D object understanding (Yi et al., 2016; Song et al., 2017). The challenge of part segmentation arises from viewpoint changes, occlusion, and lack of clear boundaries for certain parts. Existing datasets manage to alleviate the problem by enrich the data and annotations. CelebAMask-HQ (Lee et al., 2020a) is a large-scale face image dataset annotated with masks of face components. Chen et al. (2014) provides additional part segmentation upon PASCAL VOC dataset (Everingham et al., 2010). Those datasets meet the demands of latest data-driven and deep neural network based method (Lee et al., 2020b; Wang et al., 2015; Wang & Yuille, 2015). However, a well-curated part segmentation dataset containing fine-grained pixel-wise annotation usually requires time-consuming manual labeling work, which holds back the development of this field. This problem also motivates the latest work (Zhang et al., 2021; Li et al., 2021; Tritrong et al., 2021) to leverage a generative model as an infinite data generator in a semi-supervised learning setting, which gain promising results.

Gradient matching Gradient matching is an important technique in meta learning (Li et al., 2018; Sariyildiz & Cinbis, 2019), which is shown to be effective in domain generalization (Li et al., 2018), zero-shot classification (Sariyildiz & Cinbis, 2019), and dataset condensation (Zhao et al., 2021; Zhao & Bilen, 2021) *etc*. Although the general principle and gradient matching loss function in our work resemble those in the above works, we are motivated to solve a totally different problem. In particular, Gradient Matching Network (GMN) (Sariyildiz & Cinbis, 2019) employs gradient matching to train a conditional generative model towards application on zero-shot classification. Dataset Condensation (DC) (Zhao et al., 2021; Zhao & Bilen, 2021) condenses a large-scale dataset into a small synthetic one with gradient matching. Our work shows that gradient matching is also an effective way to learn annotations of GAN-generated images from limited labeled examples. Moreover, in contrast to DC where the synthesized images are typically not realistic at all, our work are concerned about photo-realistic synthetic images.

3 METHOD

3.1 PRELIMINARY

Let G denote a generative model trained from a dataset $\mathcal{D}_{tot}$ without labels. G can be trained via adversarial learning (Goodfellow et al., 2014) such that it can generate photo-realistic images. The generation process is formulated as

$$(\mathbf{h}, \mathbf{x}) = G(\mathbf{z}), \quad \mathbf{z} \sim P_z \tag{1}$$

where $\mathbf{z}$ denotes a random variable drawn from a prior distribution P_z which is typically a normal distribution, $\mathbf{x}$ denotes the generated image, and $\mathbf{h}$ denotes the hidden features in G. An annotator A_ω is constructed to decode $\mathbf{h}$ into labels

$$\hat{\mathbf{y}} = A_\omega(\mathbf{h}), \tag{2}$$

where ω parameterizes the annotator. Let $\mathcal{D}_l$ denote a manually labeled dataset. Given a fixed G, our problem is to learn annotator A_ω from $\mathcal{D}_l$ such that A_ω can annotate images generated from G.

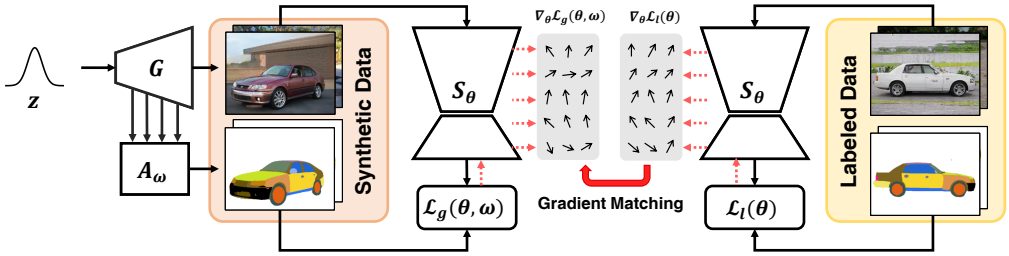

Figure 1: **Illustration** of learning to annotate with gradient matching. The procedure is as follows. (i) The gradients of segmentation network S_θ on labeled examples are computed, denoted as $\nabla_\theta \mathcal{L}_l(\theta)$. (ii) A batch of synthetic data is *randomly* generated by generator G and labeled by annotator A_ω. (iii) The gradients of S_θ on synthetic data are computed, denoted as $\nabla_\theta \mathcal{L}_g(\theta, \omega)$. (iv) Gradient matching between $\nabla_\theta \mathcal{L}_l(\theta)$ and $\nabla_\theta \mathcal{L}_g(\theta, \omega)$ is computed to optimize A_ω.

Revisiting supervised annotator learning DatasetGAN (Zhang et al., 2021) and RepurposeGAN (Tritrong et al., 2021) train annotators in a supervised learning manner. First, a set of synthetic images $\{\mathbf{x}_i\}_{i=1}^N$ generated from G are selected and annotated by humans and their generator features $\{\mathbf{h}_i\}_{i=1}^N$ are reserved. These features and manual labels $\{\mathbf{y}_i\}_{i=1}^N$ constitute the labeled dataset $\mathcal{D}_l = \{(\mathbf{x}_i, \mathbf{h}_i, \mathbf{y}_i)\}_{i=1}^N$. Second, an annotator is trained by minimizing the loss computed between annotator prediction and ground truth labels,

$$\omega = \arg\min_{\omega} \mathbb{E}_{(\cdot,\mathbf{h},\mathbf{y})\sim\mathcal{D}_l} f(A_\omega(\mathbf{h}), \mathbf{y}), \tag{3}$$

where f denotes per-pixel cross-entropy function for segmentation tasks. This method, however, requires $\mathcal{D}_l$ to be a *synthetic* and *generator-specific* set, which has the following two defects. (i) Details might be illegible in synthetic images, which increases the difficulty of annotation. (ii) Data needs to be re-labeled whenever the generator is changed. Although projecting labeled images into GAN latent space can alleviate the above drawbacks, it leads to degenerate performance due to inexact inversion (see Section C.1 in the appendix).

3.2 Learning to Annotate with Gradient Matching

Learning to learn We formulate the problem of learning A_ω as a learning-to-learn problem like Li et al. (2019); Pham et al. (2021). In particular, we introduce a segmentation network S_θ which is a deep neural network parameterized with θ. It takes as input an image and outputs a segmentation mask. This segmentation network learns the target task only from the automatically labeled generated images, which is formulated as

$$\theta^*(\omega) = \arg\min_{\theta} \underbrace{\mathbb{E}_{(\mathbf{h},\mathbf{x})=G(\mathbf{z}),\mathbf{z}\sim P_z} f(S_\theta(\mathbf{x}), A_\omega(\mathbf{h}))}_{\mathcal{L}_g(\theta,\omega)}. \tag{4}$$

where f denotes the loss function for the target task. The optimal solution of Equation 4 depends on the ω, which is therefore denoted as $\theta^*(\omega)$. The performance of learned segmentation network can be evaluated with loss on the labeled dataset $\mathcal{D}_l$ as

$$\mathcal{L}_l(\theta^*(\omega)) = \mathbb{E}_{(\mathbf{x},\mathbf{y})\in\mathcal{D}_l} f(S_{\theta^*(\omega)}(\mathbf{x}), \mathbf{y}). \tag{5}$$

The aim of learning the annotator is to produce high-quality labels such that the learned segmentation network achieve minimal loss on $\mathcal{D}_l$, which is formulated as

$$\begin{aligned} \min_{\omega} \quad & \mathcal{L}_l(\theta^*(\omega)), \\ \text{where} \quad & \theta^*(\omega) = \arg\min_{\theta} \mathcal{L}_g(\theta, \omega). \end{aligned} \tag{6}$$

This is a nested-loop optimization problem, where the inner loop optimizes segmentation network (Equation 4) and the outer loop optimizes annotator based on the solution of the inner loop. This optimization problem does not require manual labeling of generated images. To this end, any labeled images, including *real* labeled images, can serve as $\mathcal{D}_l$. While this problem can be solved with MAML-like (Finn et al., 2017) approaches (Li et al., 2019; Pham et al., 2021), its solution involves expensive unrolling of the computational graph over multiple θ states, which is memory and computation intensive. Hence, we reduce it into a simple gradient matching problem as follows. See Section C.1 in the appendix for further comparison and discussion.

Gradient matching Inspired by Li et al. (2018), we reduce the nested-loop optimization problem (Equation 6) into a gradient matching problem. First, as commonly done in gradient-based meta learning approaches, the optimization of student (Equation 4) is approximated with one-step gradient descent,

$$\theta^*(\omega) \approx \theta_0 - \eta \nabla_\theta \mathcal{L}_g(\theta_0, \omega), \tag{7}$$

where η denotes the learning rate and θ_0 denotes the initialized parameter. By plugging this equation into $\mathcal{L}_l(\theta^*(\omega))$, unfolding it as Taylor series and omitting the higher order term, we have

$$\begin{aligned} \mathcal{L}_l(\theta^*(\omega)) &\approx \mathcal{L}_l(\theta_0 - \eta \nabla_\theta \mathcal{L}_g(\theta_0, \omega)) \\ &= \mathcal{L}_l(\theta_0) - \eta \nabla_\theta^\top \mathcal{L}_l(\theta_0) \nabla_\theta \mathcal{L}_g(\theta_0, \omega) + \dots \\ &\approx \mathcal{L}_l(\theta_0) - \eta \nabla_\theta^\top \mathcal{L}_l(\theta_0) \nabla_\theta \mathcal{L}_g(\theta_0, \omega) \end{aligned} \tag{8}$$

The last approximation is conditioned on $\|\eta \nabla_\theta \mathcal{L}_g(\theta_0, \omega)\| \leq \epsilon$, where ϵ is a very small amount. By further omitting the constant term $\mathcal{L}_l(\theta_0)$ in Equation 8, we obtain the approximation of Equation 6 as

$$\min_\omega -\nabla_\theta^\top \mathcal{L}_l(\theta_0) \nabla_\theta \mathcal{L}_g(\theta_0, \omega) \qquad s.t. \ \|\eta \nabla_\theta \mathcal{L}_g(\theta_0, \omega)\| \leq \epsilon. \tag{9}$$

We notice a connection between this constrained optimization problem with the following unconstrained optimization problem

$$\min_\omega -\frac{\nabla_\theta^\top \mathcal{L}_l(\theta_0) \nabla_\theta \mathcal{L}_g(\theta_0, \omega)}{\|\eta \nabla_\theta \mathcal{L}_g(\theta_0, \omega)\|}, \tag{10}$$

where to minimize this objective, one needs to simultaneously maximize the dot product between the gradients and minimize the norm of $\nabla_\theta \mathcal{L}_g(\theta_0, \omega)$. Note that $-\frac{\nabla_\theta^\top \mathcal{L}_l(\theta_0) \nabla_\theta \mathcal{L}_g(\theta_0, \omega)}{\|\eta \nabla_\theta \mathcal{L}_g(\theta_0, \omega)\|} = \frac{\|\nabla_\theta \mathcal{L}_l(\theta_0)\|}{\eta}(1 - \frac{\nabla_\theta^\top \mathcal{L}_l(\theta_0) \nabla_\theta \mathcal{L}_g(\theta_0, \omega)}{\|\nabla_\theta \mathcal{L}_l(\theta_0)\| \|\nabla_\theta \mathcal{L}_g(\theta_0, \omega)\|}) - \frac{\|\nabla_\theta \mathcal{L}_l(\theta_0)\|}{\eta}$, and the constant term and constant coefficient can be omitted without changing the optimal solution. We re-write the learning objective of Equation 10 as

$$\mathcal{L}_{gm}(\theta_0, \omega) = D(\nabla_\theta \mathcal{L}_l(\theta_0), \nabla_\theta \mathcal{L}_g(\theta_0, \omega)) = 1 - \frac{\nabla_\theta^\top \mathcal{L}_l(\theta_0) \nabla_\theta \mathcal{L}_g(\theta_0, \omega)}{\|\nabla_\theta \mathcal{L}_l(\theta_0)\| \|\nabla_\theta \mathcal{L}_g(\theta_0, \omega)\|}, \tag{11}$$

which computes the cosine distance between the gradients of segmentation network on *automatically* labeled generated data and *manually* labeled data (see Section B in appendix for dealing with gradient matching in multi-layer neural networks). To this end, the nested-loop optimization (Equation 6) is reduced into a simple one that minimizes the gradient matching loss (Equation 11). Illustration of this procedure is presented in Figure 1.

Algorithm Note that the gradient matching problem learns an annotator for a particular network parameterized with θ_0. However, a desirable annotator should produce universal automatic labels for training *any* segmentation network with previously unseen parameters. Hence, we present an alternate training algorithm of annotator and segmentation network in Algorithm 1, where the segmentation network is iteratively updated using the automatically labeled synthetic data and the annotator is iteratively updated with gradient matching. This algorithm allows the annotator to be optimized over various segmentation network states, and therefore leads to a segmentation-network-agnostic annotator. The gradient matching problem for each segmentation network parameter is solved with K-step gradient descent and typically $K = 1$ works well in practice. Implementation details are available in the appendix (see Section B).

4 Experiments

4.1 Setup

Datasets We evaluate our method on six part segmentation datasets: **CelebA**, **Pascal-Horse**, **Pascal-Aeroplane**, **Car-20**, **Cat-16**, and **Face-34**. CelebA (Liu et al., 2015) is a large-scale human face dataset where 30,000 images are annotated with up to 19 part classes, also known as CelebAMask-HQ (Lee et al., 2020a). We consider a subset of 8 face classes and use the first 28,000 images as unlabeled set, the last 500 images as test set, and the rest 1500 images as labeled set, as in Li et al. (2021). Pascal-Horse and Pascal-Aeroplane are constructed by taking images of horse and aeroplane from PascalPart (Chen et al., 2014) which provides detailed part segmentation annotations for images

Algorithm 1: Learning to annotate with gradient matching.

Inputs :

G	trained generator
$\mathcal{D}_l$	set of labeled examples
ω, A_ω, η_a	initial annotator parameters, annotator, and learning rate for annotator
θ, S_θ, η_s	initial segmentor parameters, segmentor, and learning rate for segmentor
T, K, and B	total number of optimization steps, interval of updating segmentor, and batch size

for $t \leftarrow 1$ **to** T **do**

  // update annotator A_ω

  $\mathcal{B}_l \leftarrow \{(\mathbf{x}_i, \mathbf{y}_i) \sim \mathcal{D}_l\}_{i=1}^{B}$ // sample a batch of labeled examples

  $\nabla_\theta \mathcal{L}_l \leftarrow \frac{1}{B}\sum_{i=1}^{B} \nabla_\theta f(S_\theta(\mathbf{x}_i), \mathbf{y}_i)$ // compute gradients on $\mathcal{B}_l$

  $\mathcal{B}_g \leftarrow \{(\mathbf{x}_j, A_\omega(\mathbf{h}_j))\}_{j=1}^{B}$ // sample a batch of synthetic data

  $\nabla_\theta \mathcal{L}_g \leftarrow \frac{1}{B}\sum_{j=1}^{B} \nabla_\theta f(S_\theta(\mathbf{x}_j), A_\omega(\mathbf{h}_j))$ // compute gradients on $\mathcal{B}_g$

  $\mathcal{L}_{gm} \leftarrow D(\nabla_\theta \mathcal{L}_g, \nabla_\theta \mathcal{L}_l)$ // compute gradient matching loss

  $\omega \leftarrow \omega - \eta_a \nabla_\omega \mathcal{L}_{gm}$ // update annotator parameters

  // update segmentor S_θ

  if $t \mod K = 0$ **then**

    $\mathcal{B}_g \leftarrow \{(\mathbf{x}_j, A_\omega(\mathbf{h}_j))\}_{j=1}^{B}$ // sample a batch of synthetic data

    $\mathcal{L}_g \leftarrow \frac{1}{B}\sum_{j=1}^{B} f(S_\theta(\mathbf{x}_j), A_\omega(\mathbf{h}_j))$ // compute loss on synthetic data

    $\theta \leftarrow \theta - \eta_s \nabla_\theta \mathcal{L}_g$ // update segmentor parameters

  end

end

Output : annotator A_ω and segmentor S_θ

from Pascal VOC 2010 (Everingham et al.). The selected images are cropped according to bounding box annotations. Full process details are available in the appendix. We finally obtain 180 training images, 34 validation images, and 225 test images to constitute Pascal-Horse, and 180 training images, 78 validation images, and 269 test images to constitute Pascal-Aeroplane. In Pascal-Horse and Pascal-Aeroplane, additional images from LSUN (Yu et al., 2015) are utilized as unlabeled set. Car-20, Cat-16, and Face-34, released by Zhang et al. (2021), are three part-segmentation datasets annotated with 20, 16, and 34 part classes for car, cat, and human face, respectively. We use the same datasets to make a fair comparison to DatasetGAN (Zhang et al., 2021). In these datasets, all the training images are images generated from pre-trained StyleGAN (Karras et al., 2019) while all the test images are real images. Car-20 contains 16 training images and 10 test images; Cat-16 contains 30 training images and 20 test images; Face-34 contains 16 training images and 20 test images.

Pre-trained generators We use models of StyleGAN family (Karras et al., 2019; 2020b;a) that are either trained by ourselves or publicly available. Details are provided in the appendix (see Section B).

Evaluation We use mean intersection over union (mIoU) to evaluate the performance of segmentation networks. On CelebA, Pascal-Horse, and Pascal-Aeroplane, we use validation set to select checkpoints and report mIoU across all foreground classes, denoted as "FG-mIoU", on test set. On Car-20, Cat-16 and Face-34, we follow the setting of DatasetGAN (Zhang et al., 2021) and report the cross validation mIoU across all classes including background on test set.

4.2 Semi-Supervised Part Segmentation

Since our method has mild requirement for the labeled data, in this section, we show the effectiveness of our method under three different circumstances: real images as labeled data, synthetic images as labeled data, and out-of-domain images as labeled data.

Real images as labeled data Following SemanticGAN (Li et al., 2021), our methods are compared against SSL methods that have codes available[2], including Mean Teacher (MT) (Tarvainen & Valpola,

[2]We adopt the implementation in https://github.com/ZHKKKe/PixelSSL. For these SSL methods, the *real* unlabeled images are used as unlabeled set.

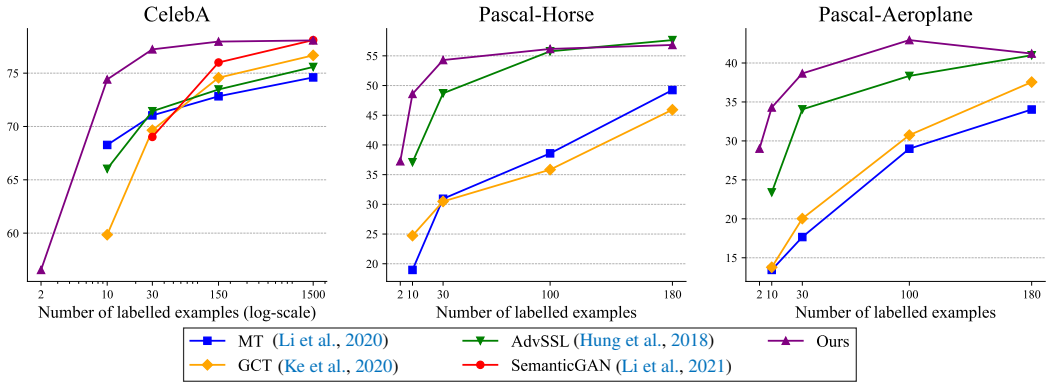

Figure 2: **Benchmark** on CelebA (*Left*), Pascal-Horse (*Middle*), and Pascal-Aeroplane (*Right*). The y-axes are FG-mIoU (%) on test set.

Methods	G	S	Cat-16 # annotations: 30 # classes: 16	Face-34 # annotations: 16 # classes: 16	Car-20 # annotations: 16 # classes: 20
TL†	-	DeepLabv3	21.58 ± 0.61	45.77 ± 1.51	33.91 ± 0.57
SSL (Mittal et al., 2019)†	-	DeepLabv3	24.85 ± 0.35	48.17 ± 0.66	44.51 ± 0.94
DatasetGAN	StyleGAN	DeepLabv3‡	32.63 ± 0.68	54.55 ± 0.25	67.53 ± 2.58
(Zhang et al., 2021)	StyleGAN	U-Net♯	31.36 ± 0.76	53.84 ± 0.41	66.27 ± 2.75
Ours	StyleGAN	DeepLabv3	33.89 ± 0.43	52.58 ± 0.61	63.55 ± 2.25
	StyleGAN	U-Net	32.64 ± 0.74	53.69 ± 0.54	60.45 ± 2.42
	StyleGAN2	DeepLabv3	33.56 ± 0.17	55.10 ± 0.39	61.21 ± 2.07
	StyleGAN2	U-Net	31.90 ± 0.75	53.58 ± 0.45	58.30 ± 2.64

Our downstream segmentation performance

	Cat-16		Face-34		Car-20	
Source \ Downstream	DeepLabv3	U-Net	DeepLabv3	U-Net	DeepLabv3	U-Net
DeepLab	33.38 ± 0.66	33.39 ± 0.74	55.11 ± 0.63	54.77 ± 0.32	63.47 ± 2.33	62.72 ± 2.89
U-Net	33.38 ± 0.40	32.42 ± 0.62	54.05 ± 0.40	53.80 ± 1.06	63.22 ± 2.42	62.25 ± 2.77

Table 1: **Comparisons to DatasetGAN** on Car-20, Cat-16, Face-34. The performance is evaluated with mIoU(%). TL: transfer learning. SSL: semi-supervised learning. †: Results taken from Zhang et al. (2021). ‡: Up-to-date performance from DatasetGAN github repository. ♯: Results obtained by ourselves using DatasetGAN source codes.

2017; Li et al., 2020), Guided Collaborative Training (GCT) (Ke et al., 2020), an adversarial-learning-based semi-supervised segmentation method (AdvSSL) (Hung et al., 2018), as well as SemanticGAN (Li et al., 2021). We benchmark performances on CelebA, Pascal-Horse, and Pascal-Aeroplane with respect to different amount of labeled data and present the results in Figure 2. Qualitative results are available in the appendix (see Figure D.7, D.8, D.9). Our method significantly outperforms other SSL methods when labeled data is extremely limited. When the number of labeled images decreases, the performance of our method drops mildly while performances of other methods decreases drastically. We attribute it to our utilization of the highly interpretable generator features. Notably, SemanticGAN (Li et al., 2021) also exploits the generative features to produce segmentation masks but its performance degrades faster than our methods as the number of labeled images decreases. We conjecture it is due to that the adversarial learning employed by SemanticGAN typically requires sufficient data to prevent discriminators from overfitting. The edges of our method become marginal under the case of large number of labels. One possible reason is that the quality of pre-trained GAN needs to be further improved, which requires more research in the future. (see Section C.5 for more discussion)

Synthetic images as labeled data We comprehensively compare our method to a supervised learning counterpart, DatasetGAN (Zhang et al., 2021) on Car-20, Cat-16, and Face-34. We follow

(a) Out-of-domain labeled examples (b) Generated images with learned annotations

Figure 3: **Cross-domain annotator learning demo.** (a) Out-of-domain labeled examples: car images and ground truth segmentations rendered from 3D CAD model. (b) Generated images with learned annotations: our method learns a reasonable annotator for GAN generated images.

the same setting as in DatasetGAN, using exactly the same synthetic images as training data. Quantitative results are presented in Table 1 and qualitative comparison is available in the appendix (see Figure D.12, D.11, D.10). First, our method achieves the same performance level with DatasetGAN on Face-34 and Cat-16. Second, as a merit of our method, we can upgrade the generator to StyleGAN2 (Karras et al., 2020b;a) without requiring extra human effort. Upgrading generator, however, brings modest improvement on Face-34 and Cat-16 and even a bit decrease on Car-20. This suggests that synthesis quality measured by metrics like FID can not precisely depict the disentanglement of generator features. Finally, our method could adapt to different segmentation architectures such as DeepLabv3 (Chen et al., 2017) and U-Net (Ronneberger et al., 2015).

We further use our trained annotator to generate synthetic segmentation datasets for training downstream segmentation networks. Table 1 shows the results when different source networks, which are used for training annotator with gradient matching, and different downstream networks are used. First, our learned synthetic datasets can be used to train downstream segmentation networks of different architecture that achieve good performances. This indicates that our learned synthetic dataset is not architecture-specific. Second, DeepLabv3 as source network generally leads to higher performances than U-Net does, suggesting that in our method the segmentation networks used for gradient matching has an impact on annotator learning.

Out-of-domain images as labeled data We further consider a challenge where out-of-domain images constitute labeled data. In particular, we render a set of car images from annotated 3D CAD models provided by CGPart[3] (Liu et al., 2021) using graphic tools (*e.g.* blender). Since 3D models are annotated with parts, the ground truth part segmentation of these rendered images are available via 3D projection. These rendered images vary in viewpoints and textures and have significant domain gap compared to realistic car images due to inexact 3D models, unrealistic textures, unnatural lighting *etc.*, raising challenges for learning annotators. Despite so, as presented in Figure 3, our method still learns reasonable annotators that produce quality segmentation labels for GAN generated images. It is noteworthy that it is nearly impossible for DatasetGAN (Zhang et al., 2021) and RepurposeGAN (Tritrong et al., 2021) to utilize such out-of-domain labeled data.

4.3 Ablation Study

The frequency of updating student The results of an ablation study w.r.t. the interval of updating student network, K, is shown in Figure 4. Experiments are run on Face-34 and Cat-16 with DeepLabv3 as segmentation network and StyleGAN as generator such that pairs of generator features and ground truth segmentation are available to quantitatively measure the performance of annotator. It shows that the annotator learns significantly faster when the segmentation network is updated more frequently. From the visualization, it can be seen that very detailed parts, *e.g.* pupils in Face-34 and eyes in Cat-16, emerge sooner if segmentation network is updated more frequently. It can be concluded that it is more effective to match gradients for various student states than optimize gradient matching for single student state.

Gradient matching on partial student parameters As the implementation of gradient matching requires maintenance of computation graph of backpropagation through student networks, one may concern the training efficiency for very deep neural networks. Here we present a simple strategy to

[3] https://qliu24.github.io/cgpart/

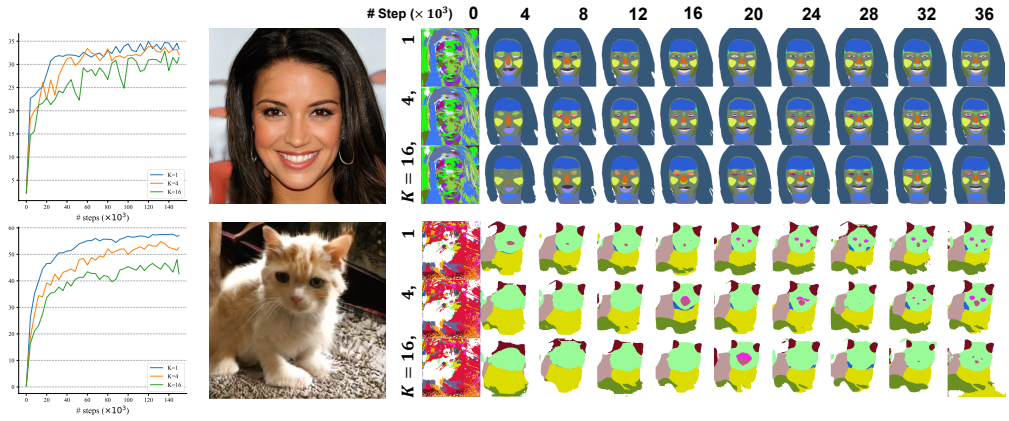

(a) Annotator performance (b) Generated Image (c) Evolution of Automatic labels

Figure 4: **Ablation study w.r.t.** K. Evolution of the learned annotator on Face-34 (first row) and Cat-16 (second row). (a) Annotator performance (mIoU (%)) on training data w.r.t. number of updating annotator steps. (b) Examples of generated images. (c) Evolution of automatic labels.

Blocks	All	Res2∼Head	Res3∼Head	Res4∼Head	Res5∼Head	* Head
Time / step	3.34×	3.34×	3.28×	3.08×	1.62×	1×
mIoU (%)	33.71 ± 0.77	34.38 ± 0.49	33.81 ± 0.99	33.78 ± 0.70	34.12 ± 0.57	33.56 ± 0.17

Table 2: **Ablation study w.r.t. blocks for matching gradients**. Evaluation is performed on Cat-16, where StyleGAN2 as generator and DeepLabv3-R101 as segmentation network. "Time / step" is measured as ratio with respect to the default setting. * denotes the default setting.

trade off the training efficiency and overall performance: gradient matching can be done only on part of student parameters. An ablation study on Cat-16 using StyleGAN2 as generator and DeepLabv3 as student network is done and the results are shown in Table 2. We consider network blocks in DeepLabv3 with ResNet-101 as backbone from bottom to top: `Res1`, `Res2`, `Res3`, `Res4` and `Res5` that are residual blocks in the backbone, and `Head` that is the segmentation head. Results show that by skipping the bottom blocks for gradient matching, the training speed is improved while the segmentation performance is affected little. We conjecture the reasons can be two folds: (i) the backbone parameters are pre-trained such that little needs to be changed during training; (ii) the gradients accumulate more randomness as they backpropagate to the bottom blocks of deep neural networks. Therefore, in practice, we only match the gradients of `Head` in DeepLabv3 by default. Additional results are available in the appendix (see Section C.3).

5 Conclusion

We propose a gradient-matching-based method to learn annotator which is able to label generated images with part segmentation by decoding the generator features into segmentation masks. Unlike existing methods that require labeling generated images for training an annotator, our method allows usage of a broader range of labeled data including realistic images, synthetic images, and even rendered images from 3D CAD models. On the benchmark of semi-supervised part segmentation, our method significantly outperform other semi-supervised segmentation methods under the circumstances of extremely limited labeled data but becomes less competitive under large-scale setting which requires feature research. The effectiveness of our method is validated on a variety of single-class datasets including well-aligned images, *e.g*. CelebA and Face-34, as well as images in the wild part of which contain cluttered backgrounds, *e.g*. Pascal-Horse, Pascal-Aeroplane, Car-20 and Cat-16. In terms of more complex scenes, discussion and investigation are further needed. With the rapid progress of generative modeling, it is promising to use more powerful generative models and explore more computer vision problems under different challenging settings in the future.

ACKNOWLEDGEMENTS

This work was supported by the National Key R&D Program of China under Grant 2018AAA0102801, National Natural Science Foundation of China under Grant 61620106005, and Beijing Municipal Science and Technology Commission grant Z201100005820005. Hakan Bilen is supported by the EPSRC programme grant Visual AI EP/T028572/1.

REPRODUCIBILITY STATEMENT

We provide all the details about the datasets, network structure, and training curriculum in the appendix. Code to reproduce our main results is publicly available at https://github.com/yangyu12/lagm.

REFERENCES

David Berthelot, Nicholas Carlini, Ekin D Cubuk, Alex Kurakin, Kihyuk Sohn, Han Zhang, and Colin Raffel. Remixmatch: Semi-supervised learning with distribution matching and augmentation anchoring. In *ICLR*, 2019a.

David Berthelot, Nicholas Carlini, Ian Goodfellow, Nicolas Papernot, Avital Oliver, and Colin A Raffel. Mixmatch: A holistic approach to semi-supervised learning. *NeurIPS*, 2019b.

Andrew Brock, Jeff Donahue, and Karen Simonyan. Large scale gan training for high fidelity natural image synthesis. In *ICLR*, 2018.

Liang-Chieh Chen, George Papandreou, Florian Schroff, and Hartwig Adam. Rethinking atrous convolution for semantic image segmentation. *arXiv preprint arXiv:1706.05587*, 2017.

Ting Chen, Simon Kornblith, Mohammad Norouzi, and Geoffrey Hinton. A simple framework for contrastive learning of visual representations. In *ICML*, 2020.

Xianjie Chen, Roozbeh Mottaghi, Xiaobai Liu, Sanja Fidler, Raquel Urtasun, and Alan Yuille. Detect what you can: Detecting and representing objects using holistic models and body parts. In *CVPR*, 2014.

Jian Dong, Qiang Chen, Xiaohui Shen, Jianchao Yang, and Shuicheng Yan. Towards unified human parsing and pose estimation. In *CVPR*, 2014.

M. Everingham, L. Van Gool, C. K. I. Williams, J. Winn, and A. Zisserman. The PASCAL Visual Object Classes Challenge 2010 (VOC2010) Results. http://www.pascal-network.org/challenges/VOC/voc2010/workshop/index.html.

Mark Everingham, Luc Van Gool, Christopher KI Williams, John Winn, and Andrew Zisserman. The pascal visual object classes (voc) challenge. *IJCV*, 2010.

Hao-Shu Fang, Guansong Lu, Xiaolin Fang, Jianwen Xie, Yu-Wing Tai, and Cewu Lu. Weakly and semi supervised human body part parsing via pose-guided knowledge transfer. *arXiv preprint arXiv:1805.04310*, 2018.

Chelsea Finn, Pieter Abbeel, and Sergey Levine. Model-agnostic meta-learning for fast adaptation of deep networks. In *ICML*, 2017.

Geoffrey French, Samuli Laine, Timo Aila, Michal Mackiewicz, and Graham Finlayson. Semi-supervised semantic segmentation needs strong, varied perturbations. In *BMVC*, 2020.

Spyros Gidaris, Praveer Singh, and Nikos Komodakis. Unsupervised representation learning by predicting image rotations. In *ICLR*, 2018.

Lore Goetschalckx, Alex Andonian, Aude Oliva, and Phillip Isola. Ganalyze: Toward visual definitions of cognitive image properties. In *ICCV*, 2019.

Ke Gong, Xiaodan Liang, Dongyu Zhang, Xiaohui Shen, and Liang Lin. Look into person: Self-supervised structure-sensitive learning and a new benchmark for human parsing. In *CVPR*, 2017.

Ian Goodfellow, Jean Pouget-Abadie, Mehdi Mirza, Bing Xu, David Warde-Farley, Sherjil Ozair, Aaron Courville, and Yoshua Bengio. Generative adversarial nets. *NeurIPS*, 2014.

Kaiming He, Haoqi Fan, Yuxin Wu, Saining Xie, and Ross Girshick. Momentum contrast for unsupervised visual representation learning. In *CVPR*, 2020.

Wei Chih Hung, Yi Hsuan Tsai, Yan Ting Liou, Yen-Yu Lin, and Ming Hsuan Yang. Adversarial learning for semi-supervised semantic segmentation. In *BMVC*, 2018.

Erik Härkönen, Aaron Hertzmann, Jaakko Lehtinen, and Sylvain Paris. Ganspace: Discovering interpretable gan controls. In *NeurIPS*, 2020.

P Izmailov, AG Wilson, D Podoprikhin, D Vetrov, and T Garipov. Averaging weights leads to wider optima and better generalization. In *UAI*, 2018.

Ali Jahanian, Lucy Chai, and Phillip Isola. On the" steerability" of generative adversarial networks. In *ICLR*, 2020.

Tero Karras, Samuli Laine, and Timo Aila. A style-based generator architecture for generative adversarial networks. In *CVPR*, 2019.

Tero Karras, Miika Aittala, Janne Hellsten, Samuli Laine, Jaakko Lehtinen, and Timo Aila. Training generative adversarial networks with limited data. In *NeurIPS*, 2020a.

Tero Karras, Samuli Laine, Miika Aittala, Janne Hellsten, Jaakko Lehtinen, and Timo Aila. Analyzing and improving the image quality of stylegan. In *CVPR*, 2020b.

Zhanghan Ke, Di Qiu, Kaican Li, Qiong Yan, and Rynson WH Lau. Guided collaborative training for pixel-wise semi-supervised learning. In *ECCV*, 2020.

Diederik P Kingma and Max Welling. Auto-encoding variational bayes. In *ICLR*, 2014.

Samuli Laine and Timo Aila. Temporal ensembling for semi-supervised learning. In *ICLR*, 2017.

Cheng-Han Lee, Ziwei Liu, Lingyun Wu, and Ping Luo. Maskgan: Towards diverse and interactive facial image manipulation. In *CVPR*, 2020a.

Cheng-Han Lee, Ziwei Liu, Lingyun Wu, and Ping Luo. Maskgan: Towards diverse and interactive facial image manipulation. In *CVPR*, 2020b.

Dong-Hyun Lee et al. Pseudo-label: The simple and efficient semi-supervised learning method for deep neural networks. In *ICML workshop*, 2013.

Da Li, Yongxin Yang, Yi-Zhe Song, and Timothy M Hospedales. Learning to generalize: Meta-learning for domain generalization. In *AAAI*, 2018.

Daiqing Li, Junlin Yang, Karsten Kreis, Antonio Torralba, and Sanja Fidler. Semantic segmentation with generative models: Semi-supervised learning and strong out-of-domain generalization. In *CVPR*, 2021.

Wei-Hong Li, Chuan-Sheng Foo, and Hakan Bilen. Learning to impute: A general framework for semi-supervised learning. *arXiv preprint arXiv:1912.10364*, 2019.

Xiaomeng Li, Lequan Yu, Hao Chen, Chi-Wing Fu, Lei Xing, and Pheng-Ann Heng. Transformation-consistent self-ensembling model for semisupervised medical image segmentation. *TNNLS*, 2020.

Tsung-Yi Lin, Michael Maire, Serge Belongie, James Hays, Pietro Perona, Deva Ramanan, Piotr Dollár, and C Lawrence Zitnick. Microsoft coco: Common objects in context. In *ECCV*, 2014.

Tsung-Yi Lin, Piotr Dollár, Ross Girshick, Kaiming He, Bharath Hariharan, and Serge Belongie. Feature pyramid networks for object detection. In *CVPR*, 2017.

Qing Liu, Adam Kortylewski, Zhishuai Zhang, Zizhang Li, Mengqi Guo, Qihao Liu, Xiaoding Yuan, Jiteng Mu, Weichao Qiu, and Alan Yuille. Cgpart: A part segmentation dataset based on 3d computer graphics models. *arXiv preprint arXiv:2103.14098*, 2021.

Ziwei Liu, Ping Luo, Xiaogang Wang, and Xiaoou Tang. Deep learning face attributes in the wild. In *ICCV*, 2015.

Sudhanshu Mittal, Maxim Tatarchenko, and Thomas Brox. Semi-supervised semantic segmentation with high-and low-level consistency. *TPAMI*, 2019.

Takeru Miyato, Shin-ichi Maeda, Masanori Koyama, and Shin Ishii. Virtual adversarial training: a regularization method for supervised and semi-supervised learning. *TPAMI*, 2018.

Xuecheng Nie, Jiashi Feng, and Shuicheng Yan. Mutual learning to adapt for joint human parsing and pose estimation. In *ECCV*, 2018.

Mehdi Noroozi and Paolo Favaro. Unsupervised learning of visual representations by solving jigsaw puzzles. In *ECCV*, 2016.

Yassine Ouali, Céline Hudelot, and Myriam Tami. Semi-supervised semantic segmentation with cross-consistency training. In *CVPR*, 2020.

Deepak Pathak, Philipp Krahenbuhl, Jeff Donahue, Trevor Darrell, and Alexei A Efros. Context encoders: Feature learning by inpainting. In *CVPR*, 2016.

Hieu Pham, Zihang Dai, Qizhe Xie, and Quoc V Le. Meta pseudo labels. In *CVPR*, 2021.

Antoine Plumerault, Hervé Le Borgne, and Céline Hudelot. Controlling generative models with continuous factors of variations. In *ICLR*, 2020.

Olaf Ronneberger, Philipp Fischer, and Thomas Brox. U-net: Convolutional networks for biomedical image segmentation. In *MICCAI*, 2015.

Mert Bulent Sariyildiz and Ramazan Gokberk Cinbis. Gradient matching generative networks for zero-shot learning. In *CVPR*, 2019.

Yujun Shen, Jinjin Gu, Xiaoou Tang, and Bolei Zhou. Interpreting the latent space of gans for semantic face editing. In *CVPR*, 2020.

Jamie Shotton, Andrew Fitzgibbon, Mat Cook, Toby Sharp, Mark Finocchio, Richard Moore, Alex Kipman, and Andrew Blake. Real-time human pose recognition in parts from single depth images. In *CVPR*, 2011.

Dylan Sisson. Pixar one twenty eight. https://renderman.pixar.com/pixar-one-twenty-eight, 2018.

Kihyuk Sohn, David Berthelot, Nicholas Carlini, Zizhao Zhang, Han Zhang, Colin A Raffel, Ekin Dogus Cubuk, Alexey Kurakin, and Chun-Liang Li. Fixmatch: Simplifying semi-supervised learning with consistency and confidence. *NeurIPS*, 2020.

Yafei Song, Xiaowu Chen, Jia Li, and Qinping Zhao. Embedding 3d geometric features for rigid object part segmentation. In *ICCV*, 2017.

Nurit Spingarn-Eliezer, Ron Banner, and Tomer Michaeli. Gan steerability without optimization. *ICLR*, 2021.

Antti Tarvainen and Harri Valpola. Mean teachers are better role models: Weight-averaged consistency targets improve semi-supervised deep learning results. In *NeurIPS*, 2017.

Nontawat Tritrong, Pitchaporn Rewatbowornwong, and Supasorn Suwajanakorn. Repurposing gans for one-shot semantic part segmentation. In *CVPR*, 2021.

Stavros Tsogkas, Iasonas Kokkinos, George Papandreou, and Andrea Vedaldi. Deep learning for semantic part segmentation with high-level guidance. *arXiv preprint arXiv:1505.02438*, 2015.

Andrey Voynov and Artem Babenko. Unsupervised discovery of interpretable directions in the gan latent space. In *ICML*, 2020.

Jianyu Wang and Alan L Yuille. Semantic part segmentation using compositional model combining shape and appearance. In *CVPR*, 2015.

Peng Wang, Xiaohui Shen, Zhe Lin, Scott Cohen, Brian Price, and Alan L Yuille. Joint object and part segmentation using deep learned potentials. In *ICCV*, 2015.

Fangting Xia, Peng Wang, Xianjie Chen, and Alan L Yuille. Joint multi-person pose estimation and semantic part segmentation. In *CVPR*, 2017.

Yi Yang and Deva Ramanan. Articulated pose estimation with flexible mixtures-of-parts. In *CVPR*, 2011.

Li Yi, Vladimir G Kim, Duygu Ceylan, I-Chao Shen, Mengyan Yan, Hao Su, Cewu Lu, Qixing Huang, Alla Sheffer, and Leonidas Guibas. A scalable active framework for region annotation in 3d shape collections. *ToG*, 2016.

Fisher Yu, Ari Seff, Yinda Zhang, Shuran Song, Thomas Funkhouser, and Jianxiong Xiao. Lsun: Construction of a large-scale image dataset using deep learning with humans in the loop. *arXiv preprint arXiv:1506.03365*, 2015.

Xiaohua Zhai, Avital Oliver, Alexander Kolesnikov, and Lucas Beyer. S4l: Self-supervised semi-supervised learning. In *ICCV*, 2019.

Yuxuan Zhang, Huan Ling, Jun Gao, Kangxue Yin, Jean-Francois Lafleche, Adela Barriuso, Antonio Torralba, and Sanja Fidler. Datasetgan: Efficient labeled data factory with minimal human effort. In *CVPR*, 2021.

Bo Zhao and Hakan Bilen. Dataset condensation with differentiable siamese augmentation. In *ICML*, 2021.

Bo Zhao, Konda Reddy Mopuri, and Hakan Bilen. Dataset condensation with gradient matching. In *ICLR*, 2021.

Yifan Zhao, Jia Li, Yu Zhang, Yafei Song, and Yonghong Tian. Ordinal multi-task part segmentation with recurrent prior generation. *TPAMI*, 2019.

Xiaojin Jerry Zhu. Semi-supervised learning literature survey. 2005.

A Dataset Details

CelebA Following Li et al. (2021), we only consider 8 part classes: background, ear, eye, eyebrow, skin, hair, mouth, and nose. The protocol for merging the 19 part classes into 8 classes is presented in Table A.1(Left). CelebAMask-HQ contains 30,000 annotated images in total. We split this dataset into unlabeled set, training set, validation set and test set as in Table A.1(Right).

8 classes	19 classes
background	background, hat, ear_r, neck_l, neck, cloth
ear	l_ear, r_ear
eye	l_eye, r_eye
eyebrow	eyebrow
skin	rest
hair	hair
mouth	mouth, u_lip, r_lip
nose	nose

Split	Image id
Unlabeled set	1∼28,000
Training set (2)	28,001∼28,002
Training set (10)	28,001∼28,010
Training set (30)	28,001∼28,030
Training set (150)	28,001∼28,150
Training set (1500)	28,001∼29,500
Validation set	27,501∼28,000
Test set	29,501∼30,000

Table A.1: *Left*: Protocol for merging part classes on CelebA. *Right*: Dataset split on CelebA.

Pascal-Horse & Pascal-Aeroplane Pascal Part (Chen et al., 2014) provides part segmentation annotations of 20 object classes for images in Pascal VOC 2010. Following other work on part segmentation (Tsogkas et al., 2015; Zhao et al., 2019; Tritrong et al., 2021), we merge the fine-grained part classes into 6 classes for horse and aeroplane. The merging protocol is presented in Table A.2. We crop the image patches that contain the object of interest according to bounding box annotations. Concretely, bounding boxes that have IoU greater than 0.05 with other boxes or empty annotations are discarded to ensure single object appears in single image patch. The patches that have any side less a certain number of pixels (32 for horse; 50 for aeroplane) are also abandoned. The crop regions are extended from bounding boxes to square boxes and the regions outside images are padded with zero. These processed patches are finally resized to 256×256 resolution to serve the training and evaluation process. For horse and aeroplane, We further split the patches in official VOC 2010 `train` split in *training* and *validation* set, and take the patches in official VOC 2010 `val` split as *test* set. This procedure finally provides 180 images as training set (*i.e.* labeled set), 33 images as validation set, and 223 images as test set in Pascal-Horse, and 180 images as labeled set, 78 images as validation set and 266 images as test set in Pascal-Aeroplane. As unlabeled images, we center-crop the 200,000 images in the large-scale LSUN (Yu et al., 2015) archive and resize them to 256×256 resolution for both horse and aeroplane.

Pascal-Horse	
6 classes	fine-grained classes
background	background
head	head, leye, reye, lear, rear, muzzle
torso	torso
legs	lfho, rfho, lbho, rbho, lfuleg, lflleg, rfuleg
neck	neck
tail	tail

Pascal-Aeroplane	
6 classes	fine-grained classes
background	background
body	body
stern	stern, tail
wing	lwing, rwing
engine	engine_{d}
wheel	wheel_{d}

Table A.2: Protocol for merging part classes on Pascal Part.

CGPart As a part segmentation dataset composed of 3D CAD models from 5 vehicle categories with 3D part manual annotations, CGPart (Liu et al., 2021) manage to render a large amount of image dataset with part mask labels by adopting blender, a well-known graphical software. In this paper, we select category *car* as training and evaluation dataset and make moderate modifications upon the rendering pipeline. Parts are merged into 15 classes, where excessively fine-grained parts that seldom emerge are combined together to avoid sample imbalance. Part merging protocol is presented in Table A.3. Viewpoints are sampled around the object with azimuth ranged in full 360°. Elevation angle is varied from 0° to 80°, yet higher sampling probability is assigned to interval $[0^\circ, 30^\circ]$. The distance

from object to viewpoint is carefully set so that the object is located at center and full in frame. Random color is painted upon the object and random texture sampled from COCO dataset (Lin et al., 2014) and Pixar-One-Twenty-Eight (Sisson, 2018) is rendered on the ground and the surroundings. $4,000$ images of 512×384 are rendered as full train dataset. When training, only $1,000$ of them in total are randomly sampled as official trainset. The original `val` split of CGPart is adopted as *test* dataset, consisting of 40 images. Test masks are merged under the same merging protocol in inference and evaluation phases.

CGPart-Car	
15 classes	fine-grained classes
background	background
back_bumper	back_bumper
car_body	left_frame, right_frame
door	back_left_door, back_right_door, front_left_door, front_right_door
front_bumper	front_bumper
head_light	left_head_light, right_head_light
hood	hood
licence_plate	back_license_plate, front_license_plate
mirror	left_mirror, right_mirror
roof	roof
tail_light	left_tail_light, right_tail_light
trunck	trunck
wheel	back_left_wheel, back_right_wheel, front_left_wheel, front_right_wheel
window	back_left_window, back_right_window, front_left_window, front_right_window, left_quarter_window, right_quarter_window
windshield	back_windshield, front_windshield

Table A.3: Protocol for merging part classes on CGPart.

B Implementation Details

Gradient matching loss Following DC (Zhao et al., 2021), the distance between gradients is measured with cosine similarity. The computation of gradient matching is quite similar as in DC. Here, we re-state this procedure for clarity. In particular, considering a multi-layer neural network S_θ that is parameterized with θ, the gradient matching loss is computed as an average over layerwise losses as $D(\nabla_\theta \mathcal{L}_l, \nabla_\theta \mathcal{L}_g) = \frac{1}{L}\sum_{i=1}^{L} d(\nabla_{\theta^{(i)}} \mathcal{L}_l, \nabla_{\theta^{(i)}} \mathcal{L}_g)$, where i denotes the layer index, L denotes the number of layers for gradient matching and

$$d(\boldsymbol{A}, \boldsymbol{B}) = \sum_{j=1}^{N} \left(1 - \frac{\boldsymbol{A}_j \cdot \boldsymbol{B}_j}{\|\boldsymbol{A}_j\| \cdot \|\boldsymbol{B}_j\|}\right) \tag{12}$$

where $\boldsymbol{A}_j$ and $\boldsymbol{B}_j$ are flattened gradient vectors for each neural node j. The minor difference of our practice compared DC is that we average the layerwise gradient distances whereas DC sum them. It is easier to handle numerical issues by using our practice in our problem. In terms of gradient matching for normalization layers such as Batch Normalization (BN), we follow the practice of DC to ignore the gradient matching of learnable parameters in BN. The BN layer is set as *train* mode during gradient matching. We find it works well.

Pre-trained GAN We use StyleGAN family (Karras et al., 2019; 2020b;a) as our pre-trained GANs. For each dataset, We either train GANs by ourselves or use publicly available models. The training configurations or links of the pre-trained GANs are listed in Table B.4. For GANs trained by ourselves, we use the checkpoints with lowest FID in the historical ones.

Annotator structure Annotator is a neural network that takes as input the generator features and output segmentation masks. DatasetGAN (Zhang et al., 2021) and RepurposeGAN (Tritrong et al., 2021) first upsample feature maps to full resolution (resolution of output image) and then concatenate

Dataset	Version	Output resolution	Training configurations or links
CelebA	StyleGAN2-ADA	256×256	`--cfg=paper256 --mirror=True`
Pascal-Horse	StyleGAN2	256×256	stylegan2-horse-config-f.pkl
Pascal-Aeroplane	StyleGAN2	256×256	`--cfg=stylegan2 --aug=noaug`
Cat-16	StyleGAN	256×256	available in DatasetGAN repo
Cat-16	StyleGAN2	256×256	lsuncat200k-paper256-ada.pkl
Face-34	StyleGAN	512×512	available in DatasetGAN repo
Face-34	StyleGAN2-ADA	512×512	`--cfg=paper512 --mirror=True`
Car-20	StyleGAN	512×512	available in DatasetGAN repo
Car-20	StyleGAN2	512×512	stylegan2-car-config-f.pkl

Table B.4: Pretrained GANs. We use the source codes provided by Karras et al. (2020a) to train StyleGAN models: `https://github.com/NVlabs/stylegan2-ada-pytorch`. For CelebA and Face-34 the StyleGAN-ADA is trained on CelebAHQ-Mask 28k images at 256×256 and 512×512 resolution, respectively. For Pascal-Aeroplane, the StyleGAN2 is trained on 200k images from LSUN airplane.

these feature maps along channel. This procedure results in extremely high-dimensional feature vectors for every pixel. These features are fed into either a pixelwise multiple layer perceptrons (MLPs) as in DatasetGAN (Zhang et al., 2021) or a convolutional neural networks (CNNs) as in (Tritrong et al., 2021). Nonetheless, this practice consumes a lot of GPU memory and run painfully slow even on high-end modern GPUs. That is also why DatasetGAN cannot consume all image feature vectors in a batch during training.

Therefore, to make training annotator more efficient, as commonly done in segmentation or detection network architectures, we fuse the multi-scale feature maps with a feature pyramid network (FPN) (Lin et al., 2017) structure and decode the fused features into segmentation masks with consecutive convolutional layers. This FPN structure saves a lot of GPU memories and computation, which allows us to consume multiple full images in one mini-batch during training. An illustration of our annotator structure is presented in Figure B.1. For generator features that are fed into annotator, we use outputs of all convolutional layers in StyleGAN as in DatasetGAN (Zhang et al., 2021) and use outputs of all synthesis blocks, each of which typically contains two consecutive convolutional layers, in StyleGAN2.

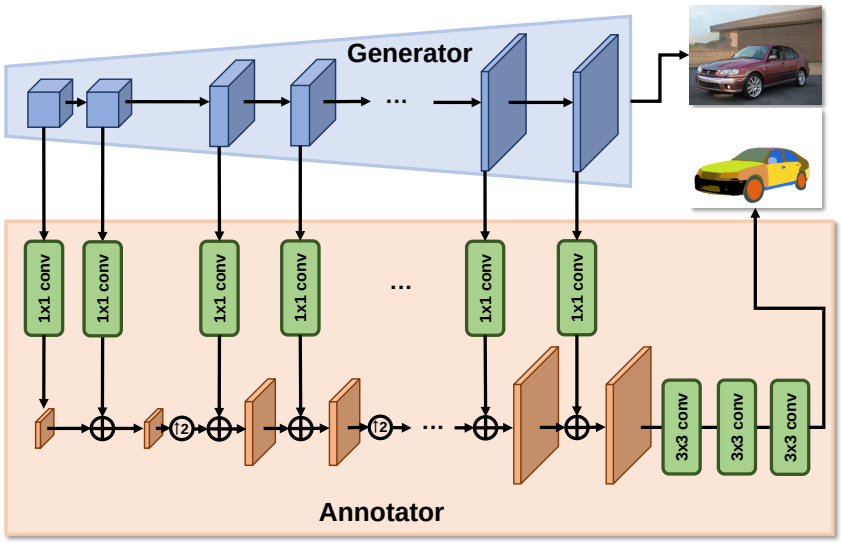

Figure B.1: Annotator architecture.

Segmentation network structures In our experiments, we employ two prevalent segmentation network structures: U-Net (Ronneberger et al., 2015) and DeepLabv3 (Chen et al., 2017) with ResNet-101 pretrained on ImageNet as backbone. For U-Net, we reference the implementation from https://github.com/milesial/Pytorch-UNet and train it from scratch on target datasets. For DeepLabv3, we use the the built-in implementation in PyTorch library[4]. For all the experiments on CelebA, Pascal-Horse, and Pascal-Aeroplane, we report the results (Figure 2) using DeepLabv3 as segmentation networks.

Training details of our method We use pixelwise cross entropy loss as $f(\cdot,\cdot)$ for training student network and computing gradients. Both the annotator and the student are optimized with SGD optimizer with learning rate 0.001 and momentum 0.9. By default, we jointly train an annotator and a student with $K = 1$ and batch size 2 for $150,000$ steps.

Training details of competing semi-supervised methods For MT, GCT and AdvSSL, we train the networks for $10,000$ iterations with batch size 16 for labeled data and 8 for unlabeled data. Learning rate is decayed with power 0.9 every iteration. During training process, the input images are randomly resized to a scale in $[160, 640]$ and cropped to 256×256. For the rest of the hyper-parameters, we use the default settings as in PixelSSL.

C Further Analysis

C.1 Comparison to Other Baselines

Inversion baseline One way to make the supervised learning of annotator be able to utilize existing labeled images is to (i) project images into GAN latent space to acquire generator features, (ii) use the joint generator features and ground truth labels to train an annotator. We call this method "inversion baseline". We evaluate the performance of this method on Cat-16, Face-34, and Car-20 using StyleGAN2 as generator and make a comparison to our method in Table C.5. Concretely, we first use the projection method provided by Karras et al. (2020b) to compute the latent style codes that result in a reconstruction of labeled images. Second, the latent style codes are forwarded to the generator to acquire generator features. We present examples of such reconstruction in Figure C.2 which shows that the reconstruction is quite accurate. However, the performance of inversion baseline fails to combat our method and the automatic labels for a randomly generated image are of low quality (see Figure C.3). We argue that it is non-trivial to inverse the GAN generation process to acquire features for specific images. Even though the reconstruction of images is satisfying, one is still unable to exactly recover the generator features, which leads to an degraded learning of annotator.

Methods	G	S	Cat-16	Face-34	Car-20
Ours	StyleGAN2	DeepLab	33.56 ± 0.17	55.10 ± 0.39	61.21 ± 2.07
	StyleGAN2	U-Net	31.90 ± 0.75	53.58 ± 0.45	58.30 ± 2.64
Inversion baseline	StyleGAN2	DeepLab	15.14 ± 0.27	47.87 ± 0.86	52.18 ± 2.31
	StyleGAN2	U-Net	12.78 ± 0.42	48.57 ± 0.38	52.41 ± 1.69

Table C.5: Comparison of our methods to inversion baseline.

Pseudo-labeling baseline Another way to employ existing labeled images to train an annotator in supervised learning manner is to use a trained segmentation model to predict pseudo labels for the generated images. We refer to this method as "pseudo-labeling baseline". In particular, this baseline method involves three stages: (i) a segmentation model is trained on the labeled data; (ii) the trained segmentation model is used to produce pseudo labels for every random image generated from generator, which further supervise the learning of an annotator; (iii) the joint generator and trained annotator are used for generating automatically labeled data which is further used for training a downstream segmentation network.

As shown in Table C.6, pseudo-labeling baseline performs badly, especially on Car-20, which can be accounted for the following reasons. Our method can be understood as distilling knowledge from a

[4] https://pytorch.org/hub/pytorch_vision_deeplabv3_resnet101/

Figure C.2: Examples of reconstruction quality. The first row shows target images and the second row shows the reconstructed images.

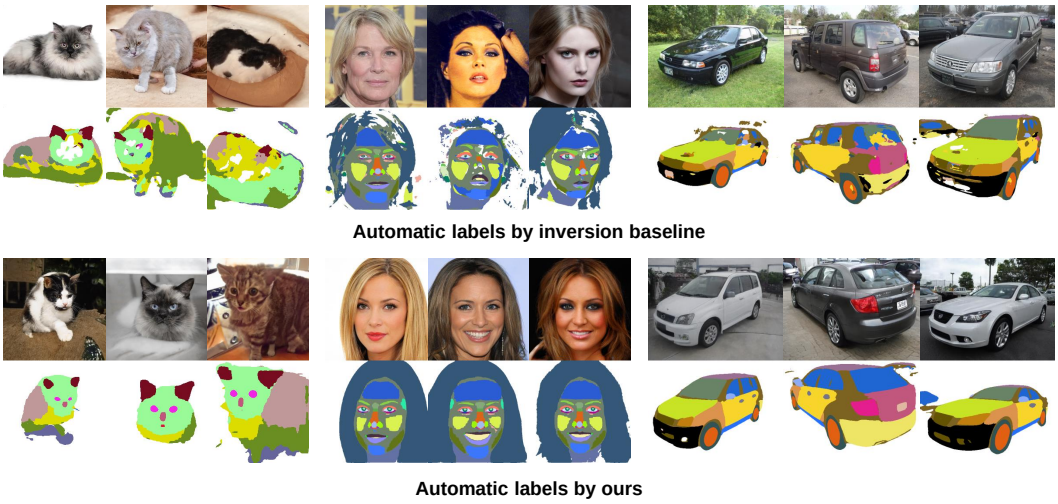

Figure C.3: Comparison of the automatic labels produced by inversion baseline v.s. ours.

generative model to a discriminative model, whereas this pseudo-labeling baseline is more like the other way around – distilling knowledge from a discriminative model to a generative model. The highly interpretable generator features make our method possible to learn annotations from only a few labeled data. In contrast, the discriminative model can hardly learn to acquire valuable knowledge from extremely limited labeled data.

Methods	G	S	Cat-16	Face-34	Car-20
Ours	StyleGAN2	DeepLab	33.56 ± 0.17	55.10 ± 0.39	61.21 ± 2.07
	StyleGAN2	U-Net	31.90 ± 0.75	53.58 ± 0.45	58.30 ± 2.64
Pseudo-labeling baseline	StyleGAN2	DeepLab	20.21 ± 0.65	42.15 ± 0.68	12.37 ± 0.91
	StyleGAN2	U-Net	16.72 ± 0.79	43.26 ± 1.20	13.48 ± 0.48

Table C.6: Comparison of our methods to pseudo-labeling baseline.

Our method with MAML One direct solution to Equation 6 is to use MAML-like algorithm, which unrolls the inner loop with multi-step stochastic gradient descent, reserves the computation graph, computes the meta loss, and finally backpropagates the gradients for updating the annotator. We refer to this baseline as "Ours-K-step-MAML" and summarize this algorithm as Algorithm 2. Table C.7 shows the experimental comparison of gradient matching versus MAML, where we use $\eta_i = 0.1$ in MAML for all experiments. The following conclusions can be drawn from these results. First, gradient matching generally leads to higher performance and obtains more consistent results across different datasets and different segmentation network architectures than MAML. Second, MAML probably requires multiple inner-loop steps (more than two) to match the performance of gradient matching, given that it fails to do so with two inner-loop steps. This is very inefficient and requires huge computation resources. Furthermore, in practice, we observe that MAML appears unstable and sensitive to hyperparameters (*e.g.* inner-loop learning rate) across different datasets and

different network architectures, whereas gradient matching nearly requires neither dataset-specific nor network-architecture-specific hyperparameters.

Algorithm 2: Learning to annotate with K-step MAML.

Inputs :

G	trained generator
$\mathcal{D}_l$	set of labeled examples
ω, A_ω, η_ω	initial annotator parameters, annotator, and learning rate for annotator
θ, S_θ, η_θ	initial segmentor parameters, student, and learning rate for student
T and B	total number of optimization steps and batch size
η_i and K	inner-loop learning rate and inner-loop steps

for $t \leftarrow 1$ **to** T **do**
  // update annotator A_ω
  $\theta' \leftarrow \theta$ // copy segmentor parameters for simulated SGD
  $\mathcal{B}_g \leftarrow \{(\mathbf{x}_j, A_\omega(\mathbf{h}_j))\}_{j=1}^{B}$ // sample a batch of synthetic data
  for $k \leftarrow 1$ **to** K **do**
    $\nabla_{\theta'}\mathcal{L}_g \leftarrow \frac{1}{B}\sum_{j=1}^{B}\nabla_{\theta'} f(S_{\theta'}(\mathbf{x}_j), A_\omega(\mathbf{h}_j))$ // compute gradients on $\mathcal{B}_g$
    $\theta' \leftarrow \theta' - \eta_i \nabla_{\theta'}\mathcal{L}_g$ // update segmentor parameters
  end
  $\mathcal{B}_l \leftarrow \{(\mathbf{x}_i, \mathbf{y}_i) \sim \mathcal{D}_l\}_{i=1}^{B}$ // sample a batch of labeled examples
  $\mathcal{L}_l \leftarrow \frac{1}{B}\sum_{i=1}^{B} f(S_\theta(\mathbf{x}_i), \mathbf{y}_i)$ // compute meta loss
  $\omega \leftarrow \omega - \eta_\omega \nabla_\omega \mathcal{L}_l$ // update annotator parameters

  // update segmentor S_θ
  $\mathcal{B}_g \leftarrow \{(\mathbf{x}_j, A_\omega(\mathbf{h}_j))\}_{j=1}^{B}$ // sample a batch of synthetic data
  $\mathcal{L}_g \leftarrow \frac{1}{B}\sum_{j=1}^{B} f(S_\theta(\mathbf{x}_j), A_\omega(\mathbf{h}_j))$ // compute loss on synthetic data
  $\theta \leftarrow \theta - \eta_\theta \nabla_\theta \mathcal{L}_g$ // update segmentor parameters
end

Output : annotator A_ω and segmentor S_θ

Methods	G	S	Cat-16 # annotations: 30 # classes: 16	Face-34 # annotations: 16 # classes: 16	Car-20 # annotations: 16 # classes: 20
Ours-GM	StyleGAN	DeepLab	33.89 ± 0.43	52.58 ± 0.61	63.55 ± 2.25
	StyleGAN	U-Net	32.64 ± 0.74	53.69 ± 0.54	60.45 ± 2.42
	StyleGAN2	DeepLab	33.56 ± 0.17	55.10 ± 0.39	61.21 ± 2.07
	StyleGAN2	U-Net	31.90 ± 0.75	53.58 ± 0.45	58.30 ± 2.64
Ours-1-step-MAML	StyleGAN	DeepLab	32.49 ± 0.43	35.24 ± 0.20	54.74 ± 2.67
	StyleGAN	U-Net	16.70 ± 0.43	23.21 ± 0.07	29.26 ± 0.72
	StyleGAN2	DeepLab	30.30 ± 0.53	33.82 ± 0.24	54.42 ± 3.11
	StyleGAN2	U-Net	22.78 ± 0.65	32.64 ± 0.18	26.59 ± 0.60
Ours-2-step-MAML	StyleGAN	DeepLab	32.98 ± 0.50	39.73 ± 0.13	58.22 ± 2.17
	StyleGAN2	DeepLab	29.66 ± 0.69	39.04 ± 0.23	56.47 ± 2.32

Table C.7: Comparisons of our methods using gradient matching (GM) versus MAML on Car-20, Cat-16, Face-34 with different network architectures. The performance is evaluated with mean intersection over union (mIoU(%)) across all part classes plus a background class.

C.2 The Impact of Student States

As we present an alternate learning algorithm between annotator and student, we study the impact of updating student states. In particular, we investigate the training convergence and overall performance of annotator when different series of student states are employed for gradient matching. We present in Figure C.4 & Figure C.5 the evolution of annotator performance evaluated on training set during training process, where "baseline" denotes the default setting and the following settings are further compared. (i) The student parameters are randomly re-initialized rather than learned from generated

images, denoted as "random re-init". (ii) The student is pretrained to acquire a fair performance ($\sim 40.7\%$ mIoU evaluated on test set), denoted as "pre-trained". (iii) The student is a DeepLabv3 network that has backbone randomly initialized rather than pretrained on ImageNet, denoted as "scratch". (iv) The student parameters, either randomly initialized or pre-trained, are fixed, denoted as "random init & fixed" and "pre-trained & fixed", respectively.

First, "Fixed" students result in a gradient matching problem on single student state, which learns annotator with very poor performance compared to the default setting. This result suggests that matching gradients for a series of student states is vital to learning annotator. Second, even though it is crucial to require annotator to produce student-agnostic labels, a randomly re-initialization strategy does not work well (see results of "random re-init" v.s. "baseline"). Moreover, the results of "pre-trained & fixed" is better than "random init & fixed", which suggest that a well-performed student provides more informative gradients such that by gradient matching the annotator can be more effectively learned. Third, the conclusion that a well-performed student provides more informative gradients can be further verified by the fact that matching gradients of pre-trained students accelerates the learning of annotator (see results of "baseline" v.s. "pre-trained" and "baseline" v.s. "scratch").

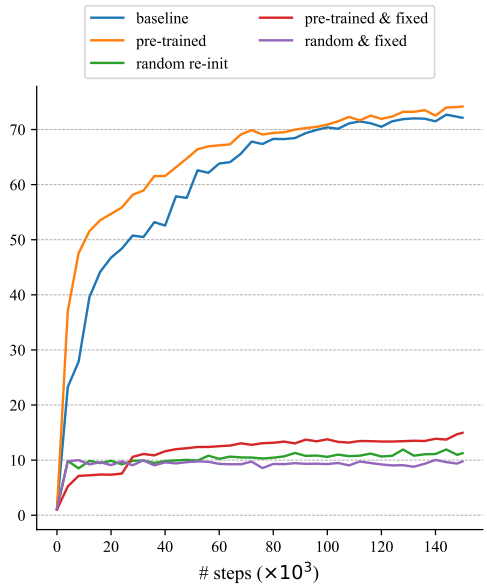

Figure C.4: Comparison of the training convergence under different settings of sampling segmentation network states. Annotator performance (mIoU (%)) is evaluated on training set of Car-20. Segmentation network is U-Net.

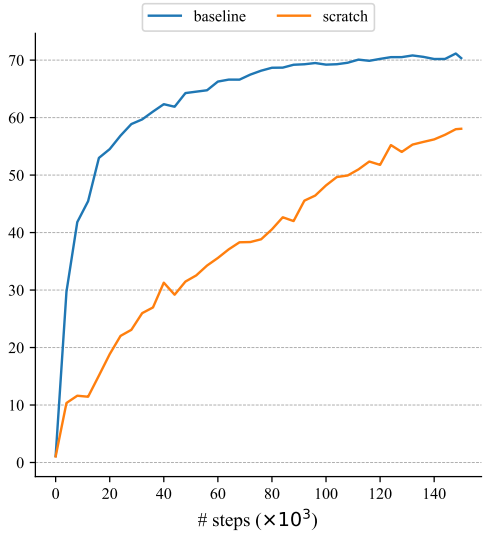

Figure C.5: Comparison of the training convergence of segmentation network with pretrained backbone ("baseline") versus segmentation network with randomly initialized backbone ("scratch"). Annotator performance (mIoU (%)) is evaluated on training set of Car-20. Segmentation network is DeepLabv3-R101.

C.3 Trade off Training Efficiency with Performance

Gradient matching on partial network parameters We present additional results on in Table C.8. U-Net takes as input an image and first produce feature map at multiple downsampled scales with consecutive convolutional and pooling layers. These feature maps are then processed by consecutive convolutional and upsampling layers to be mapped back to original input scale. Notably, skip connection is employed to connect the multi-scale feature maps along the downsampling path and upsampling path. We consider the following particular group of layers in U-Net: (i) `Up` v.s. `Down`, (ii) `Input` v.s. `Output`, and (iii) `U1` v.s. `U2`. `Up` and `Down` denote the convolutional layers along the upsampling and downsampling path, respectively. `Input` and `Output` denote the input convolutional layer and the output convolutional layer, respectively. `U1` and `U2` denote the convolutional layers that process feature maps at $1/1$ and $1/2$ scales, respectively. From the results

we can see that matching gradients of layers near the output end is more effective than doing so at layers near the input end.

Blocks	* All	Up	Down	Input	Output	U1	U2
Time / step	1×	0.65×	0.73×	0.73×	0.34×	0.71×	0.63×
mIoU (%)	31.90 ±0.75	30.12 ±0.43	14.42 ±0.23	12.40 ±0.40	25.41 ±0.77	30.18 ±0.79	31.22 ±0.48

Table C.8: **Ablation study w.r.t. blocks for matching gradients** on U-Net. Evaluation is performed on Cat-16, where StyleGAN2 as generator. "Time / step" is measured as ratio with respect to the case of default setting. * denotes the default setting.

Resolution of input to segmentation network Another way to improve the training efficiency is to reduce the resolution of input to student network. Note that the resize operation can be implemented with interpolation which is differentiable. We show in Figure C.6 and Table C.9 that by reducing the resolution, the training speed improves significantly, but the annotator performance and downstream segmentation networks compromises. Therefore, in practice, the student resolution can be tuned by trading off the training efficiency and effectiveness.

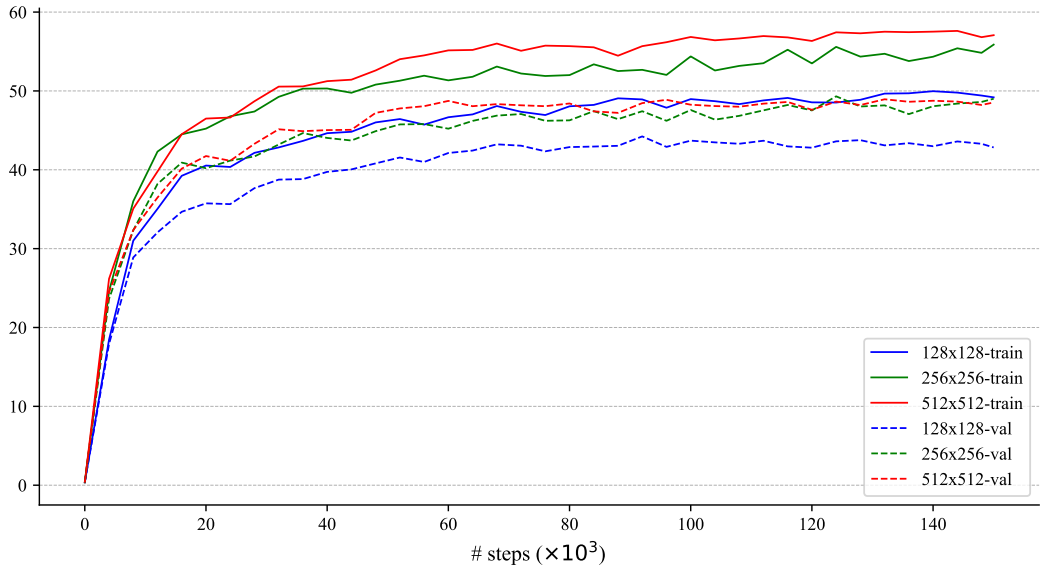

Figure C.6: The evolution of annotator performance(mIoU (%)) evaluated on training and validataion set during training process on Face-34.

Resolution	* 512 × 512	256 × 256	128 × 128
Time / step	1×	0.45×	0.37×
mIoU (%)	51.93 ± 0.28	50.71 ± 0.39	45.53 ± 0.31

Table C.9: Comparisons of the training efficiency (time / step) and downstream segmentation (U-Net) performance (mIoU) w.r.t. different input resolution to segmentation network on Face-34. "Time / step" is measured as ratio with respect to the default setting. * denotes the default setting.

C.4 The Impact of Generator

As our segmentation network is trained only on the generated images (Algorithm 1 Line 9∼11) and a very shallow network is employed to convert generator features into annotations, the segmentation performance is inevitably affected by the quality of pre-trained GANs. which suggests that the quality

of generative features significantly affect the quality of annotations. Table C.10 shows that premature GANs – ones with high FID score – generally leads to lower segmentation performance.

	CelebA				Pascal-Aeroplane			
FID ↓	10.21	6.80	5.12	4.29	11.74	7.78	6.25	5.04
FG-mIoU (%) ↑	73.92	76.61	77.48	78.07	21.69	36.01	38.81	41.21

Table C.10: The segmentation performance with respect to generators of different quality (indicated by FID) on CelebA and Pascal-Aeroplane.

C.5 Discussion on Large-Scale Setting

As shown in Fig. 2, the performance of our method begins to saturate and even beaten by other semi-supervised segmentation method when the number of labels grow large. To investigate the performance of our method under large-scale setting, we further run experiments with more unlabeled and labeled data and present the results in Table C.11. It shows that the performance of our method even slightly drops when the number of unlabeled data or the number of labels increases and is significantly beaten by supervised learning. We hypothesize the reason to be that our method is seriously limited by the performance of GANs which still struggle to fit large-scale datasets. In contrast, under large-scale setting, supervised learning becomes stronger since more labels are available. How to address this issue requires further research in the future.

Method	unlabeled data	# labels	FG-mIoU (%)
Supervised learning	–	29,000	84.32
Ours	CelebA-train (29,000)	1,500	77.90
Ours	CelebA-train (29,000)	29,000	76.03
Ours	CelebA-train + FFHQ (99,000)	29,000	75.00

Table C.11: Experiments on human face part segmentation under large-scale setting.

C.6 Comparison to DatasetGAN in Other Aspects

Real images v.s. synthetic images as labeled data Since our method removes the necessity of labeling synthetic images, we study if replacing the labeled synthetic images with real ones could improve the segmentation performance. Table C.12 shows an evaluation on CelebA-test at 512×512 resolution across 8 face classes. DatasetGAN, which uses 16 annotated synthetic images for training, achieves 70.01 mIoU performance. Our method achieves a bit higher performance when using the exactly same synthetic images as DatasetGAN. Moreover, the performance of our method can be further improved with around 6.7% mIoU by replacing the labeled synthetic images with real ones in CelebA-train. This suggests that the capability of using real labeled data exhibits the superiority of our method over DatasetGAN.

	Labeled data	CelebA-test@512×512
DatasetGAN (Zhang et al., 2021)†	Synthetic	70.01
Ours	Synthetic	72.55
	Real	79.25

Table C.12: Comparison of the performance when using synthetic images versus real images as labeled data. †: Results taken from Zhang et al. (2021).

Our method with more labeled data on Car-20 Considering our method does not match the performance of DatasetGAN on Car-20, we further investigate if this gap can be narrowed with the help of more labeled data. Table C.13 presents the performance of our method when more labeled data is used on Car-20. It shows that with increased number of labeled data, the performance of our method gradually approaches that of DatasetGAN.

G	S	DatasetGAN	Ours		
		# annotations: 16	# annotations: 16	# annotations: 25	# annotations: 33
StyleGAN	DeepLab	67.53 ± 2.58	63.55 ± 2.25	64.68 ± 2.53	64.88 ± 2.52
StyleGAN	U-Net	66.27 ± 2.75	60.45 ± 2.42	63.09 ± 3.49	65.37 ± 2.78

Table C.13: Performance of our method with respect to different number of labeled images on Car-20 dataset.

D QUALITATIVE RESULTS

Figure D.7: Qualitative results of our method on CelebA. The segmentation results of our models trained from 2, 10, and 30, 150, 1500 labeled examples are presented.

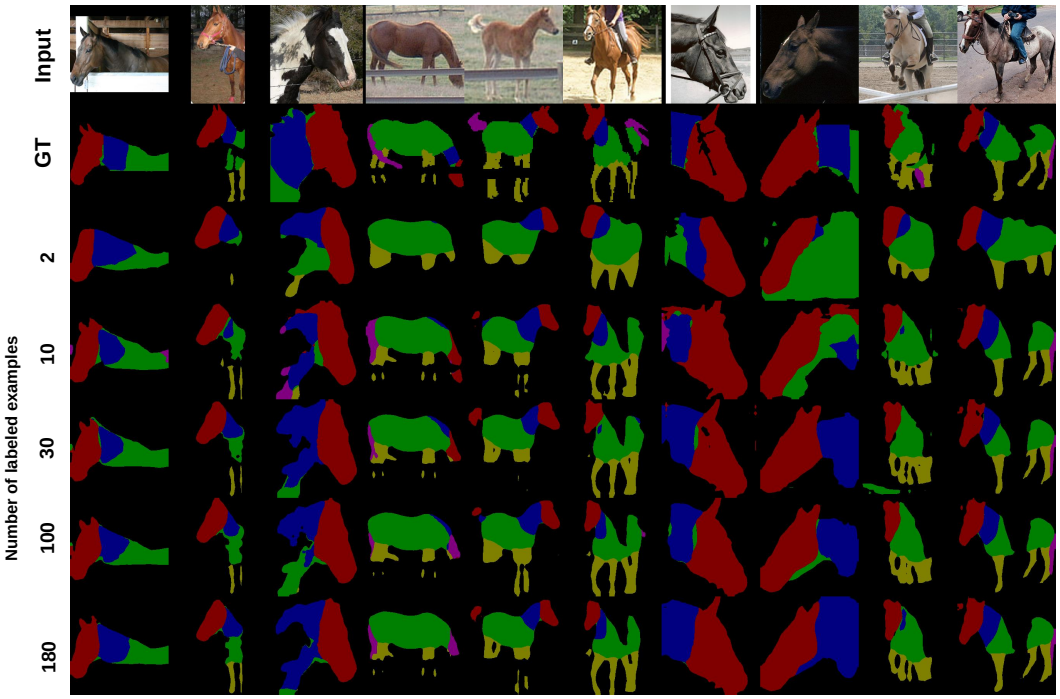

Figure D.8: Qualitative results of our method on Pascal-Horse. The segmentation results of our models trained from 2, 10, and 30, 100, 180 labeled examples are presented.

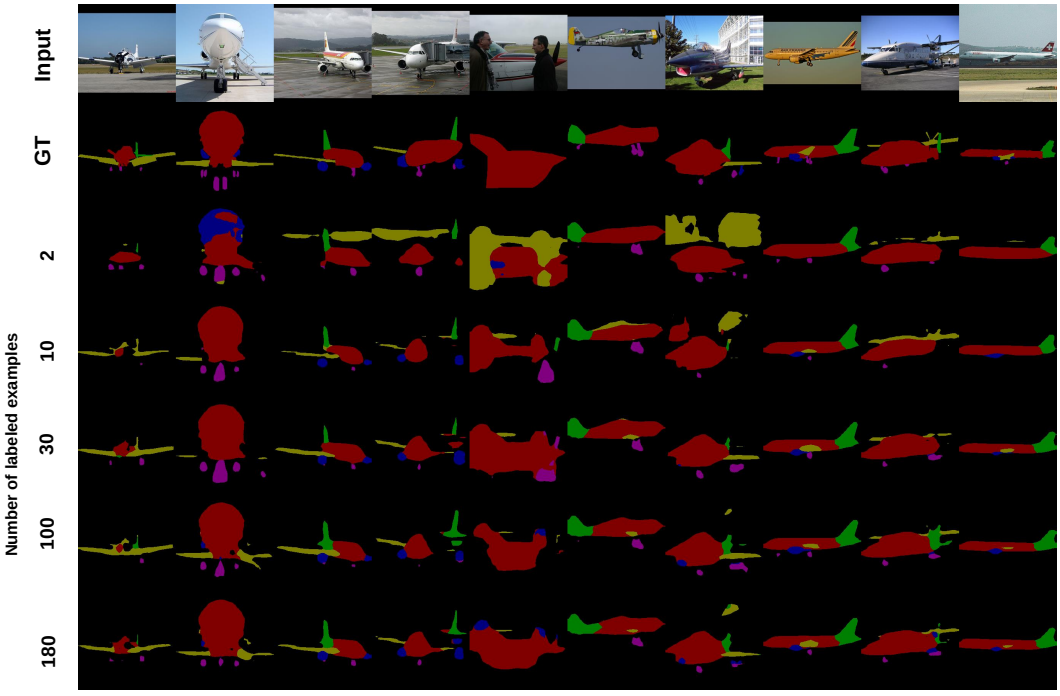

Figure D.9: Qualitative results of our method on Pascal-Aeroplane. The segmentation results of our models trained from 2, 10, and 30, 100, 180 labeled examples are presented.

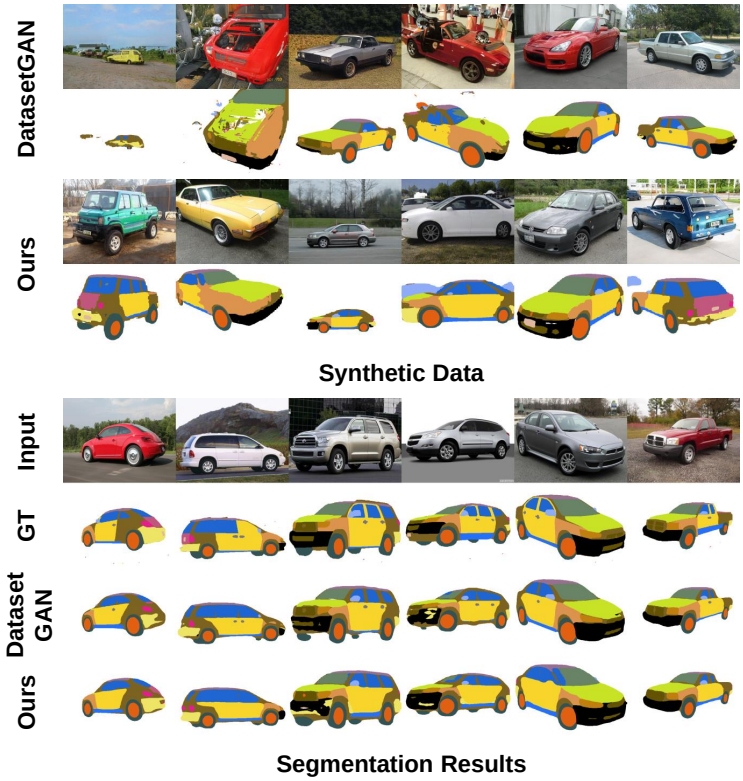

Figure D.10: Qualitative comparison of our method to DatasetGAN on Car-20

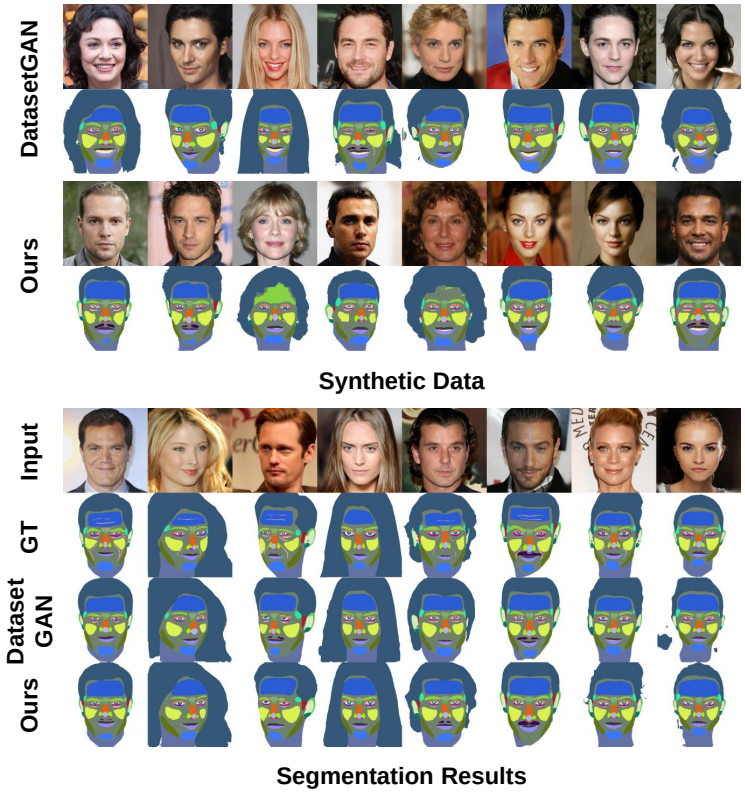

Figure D.11: Qualitative comparison of our method to DatasetGAN on Face-34.

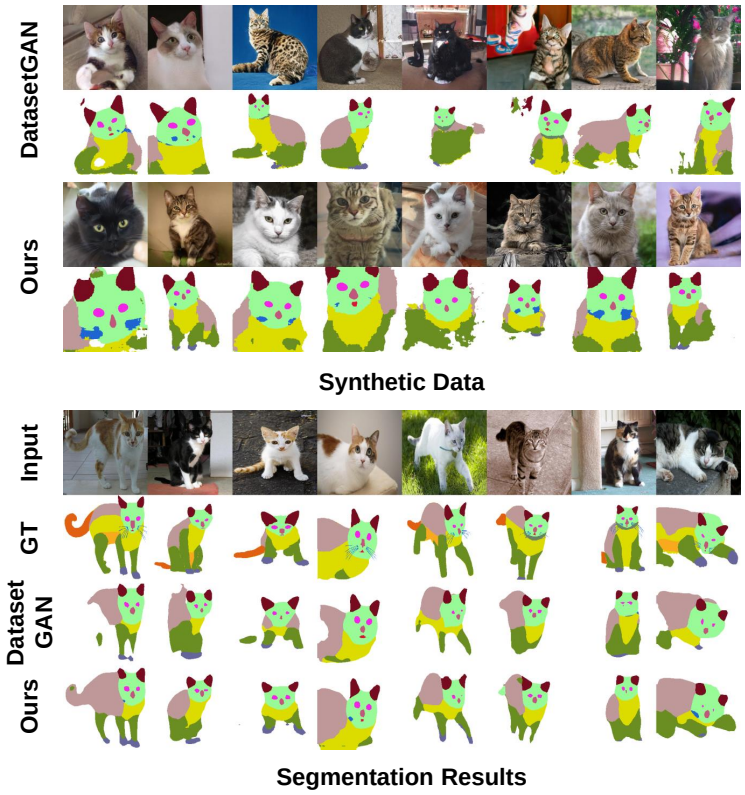

Figure D.12: Qualitative comparison of our method to DatasetGAN on Cat-16.